Available online at www.sciencedirect.com
SCIENCE DIRECT
Geochimica et Cosmochimica Acta 70 (2006) 1565–1580
Geochimica
www.elsevier.com/locate/gca

Constraints on core formation from Pt partitioning in mafic silicate liquids at high temperatures

E. Cottrell *, D. Walker

Lamont-Doherty Earth Observatory and Department of Earth and Environmental Sciences, Columbia University, Palisades, NY 10964, USA

Received 25 June 2005; accepted in revised form 14 November 2005

Abstract

A new high temperature piston cylinder design has enabled the measurement of platinum solubility in mafic melts at temperatures up to 2500 °C, 2.2 GPa pressure, and under reducing conditions for 1–10 h. These high temperature and low f_{O_2} conditions may mimic a magma ocean during planetary core formation. Under these conditions, we measured tens to hundreds of ppm Pt in the quenched silicate glass corresponding to $D_{Pt}^{met/sil} \approx 10^{3-4}$, 4–12 orders of magnitude lower than extrapolations from high f_{O_2} experiments at 1 bar and at temperatures no higher than 1550 °C. Moreover, the new experiments provide coupled textural and compositional evidence that noble metal micro-nuggets, ubiquitous in experimental studies of the highly siderophile elements, can be produced on quench: we measure equally high Pt concentrations in the rapidly quenched nugget-free peripheral margin of the silicate as we do in the more slowly quenched nugget-bearing interior region. We find that both temperature and melt composition exercise strong control on $D_{Pt}^{met/sil}$ and that Pt^0 and Pt^{1+} may contribute significantly to the total dissolved Pt such that low f_{O_2} does not imply low Pt solubility. Equilibration of metal alloy with liquid silicate in a hot primitive magma might not have depleted platinum to the extent previously believed.

1. Introduction

Wide-spread melting of metal and silicate characterizes many recent physical models for terrestrial accretion and core formation (Sasaki and Nakazawa, 1986; Benz and Cameron, 1990; Canup and Asphaug, 2001; Cameron, 2002; Yoshino et al., 2003). The extent to which metal and silicate were in equilibrium during core formation remains an unresolved issue, but one whose resolution will inform dynamic models of metal/silicate phase separation and the evolution of the early Earth (Stevenson, 1990; Karato and Murthy, 1997; Walter et al., 2000; Rubie et al., 2003; Righter, 2003; Halliday, 2004; ; Walter and Tronnes, 2004).

Metal–silicate partitioning experiments place chemical constraints on the degree to which equilibrium conditions during core formation can account for modern mantle elemental abundances. The low mantle abundances of the siderophile elements relative to chondrites likely reflects their high metal–silicate partition coefficients ($D_i^{met/sil}$, defined as the concentration ratio of the element i in the metal to that in the silicate phase by weight). Experiments performed at 1 bar and $\leqslant$1550 °C predict large mantle depletions for the moderately siderophile elements (MSE: Mo, W, Co, Ni, P, Cu, Ga) and almost complete extraction of the highly siderophile elements (HSE: Re, Os, Ir, Pt, Ru, Rh, Pd, Au) from the silicate mantle during core formation. These experiments also predict major fractionations among the MSE and HSE. We observe however, that while siderophile elements are depleted in the mantle, some subgroups have retained their chondritic ratios and have concentrations several orders of magnitude higher than those predicted by low pressure–temperature metal–silicate equilibration experiments (Ringwood, 1966, 1979).

* Corresponding author. Present address: Carnegie Institution of Washington, Geophysical Laboratory, 5251 Broad Branch Rd NW, Washington, DC 20008, USA. Fax: +1 202 478 8901.
E-mail addresses: ecottrell@gl.ciw.edu (E. Cottrell), dwalker@ldeo.columbia.edu (D. Walker).

0016-7037/$ - see front matter © 2005 Elsevier Inc. All rights reserved.
doi:10.1016/j.gca.2005.11.021

The "excess" abundances and chondritic ratios of the siderophile elements may be the result of a cold and progressively more oxidizing accretion process (e.g., Kimura et al., 1974; Wänke, 1981; O' Neill, 1991), or they may be the residual signature of an ancient magma ocean which equilibrated metal and silicate under conditions dissimilar to 1 bar and moderate temperatures (e.g., Murthy, 1991; Li and Agee, 1996; Righter et al., 1997; Walter and Tronnes, 2004). The convergence of $D_{Ni}^{met/sil}$ and $D_{Co}^{met/sil}$ with increasing pressure (Li and Agee, 1996, 2001) provides a striking example of how partitioning behavior can change with intensive parameters. While the convergence of $D_{Ni}^{met/sil}$ and $D_{Co}^{met/sil}$ has been revised based on new experiments below 3 GPa by Kegler et al. (2004, 2005), Chabot et al. (2005) demonstrate convincingly that equilibration of metal and silicate in a reducing (~2 log units below the iron–wüstite buffer) magma ocean between 30 and 60 GPa and $\geqslant$2000 °C could have set the mantle budgets of Ni and Co. These conditions also satisfy the constraints imposed by the slightly siderophile elements V, Mn, Cr (Gessmann and Rubie, 2000; Chabot and Agee, 2003) and the moderately siderophile elements P, W, Co, Ni, Mo (e.g., Righter et al., 1997; Walter et al., 2000; Righter, 2003). Thus, high pressure, high temperature, and low oxygen fugacity conditions in a putative magma ocean seem to resolve the discrepancy between observation and experiment for the majority of the slightly and moderately siderophile elements. Yet, results for the highly siderophile elements remain elusive.

1.1. HSE micro-nuggets

Almost no experimental partitioning data exist for the HSE beyond 1600 °C. Further, under reducing conditions of low oxygen fugacity (f_{O_2}) the formation of HSE "micro-nuggets" complicates interpretation of measured HSE concentrations in experimental silicates (Borisov and Palme, 1995, 1997; Lindstrom and Jones, 1996; Ertel et al., 1999; Holzheid et al., 2000).

The behavior of platinum under reducing conditions provides a canonical example of the ambiguity that arises from micro-nugget formation. Several studies on iron-free systems at low pressure and temperature but at high f_{O_2} have demonstrated that Pt concentrations in silicate decrease as f_{O_2} drops (Borisov and Palme, 1997; Ertel et al., 1999) according to

$$X_{Pt} = \tfrac{1}{2}\log(f_{O_2}) + \text{a constant}, \quad (1)$$

where X_{Pt} is the concentration by weight of Pt in silicate in equilibrium with pure Pt metal. The slope of the correlation indicates that Pt dissolves in the silicate melt as Pt^{2+} under oxidizing conditions. However, as f_{O_2} decreases to the low fugacities relevant to core formation, Pt concentrations in the silicate do not continue to fall. Instead, at low pressure and temperature, measured Pt concentrations in silicate equilibrated with Pt metal hover around 1 ppm across 8 orders of magnitude in f_{O_2}—a low concentration, but well above the detection limits of either neutron activation analysis (Borisov and Palme, 1995, 1997) or laser-ablation ICP-MS (Ertel et al., 1999). Under these conditions of low f_{O_2} and low temperature, micro-nuggets (50 nm–2 μm) of Pt are ubiquitously observed in the quenched glass causing scatter or "noise" over several orders of magnitude in measured Pt concentration—far greater than analytical noise. The micro-nuggeting phenomena has been reported for all of the HSE. As with other HSE, Pt micro-nuggets have thus far evaded all attempts to eradicate them (Borisov and Palme, 1995, 1997; Lindstrom and Jones, 1996; Ertel et al., 1999; O' Neill et al., 1995; Cottrell and Walker, 2002; Cottrell, 2004).

The loss of correlation between f_{O_2} and Pt concentration, concomitant with the appearance of micro-nuggets, leads investigators to conclude that either the micro-nuggets are some sort of contamination (Borisov and Palme, 1995, 1997; O' Neill et al., 1995; Ertel et al., 1999, 2001; Holzheid et al., 2000; Fortenfant et al., 2003), or that the metals are dissolving as a neutral species and are reappearing on quench (Cottrell and Walker, 2002, 2004). If the former, analysis of the silicate should avoid inclusion of micro-nuggets. At low metal concentrations, however, chance inclusion of micro-nuggets will dominate measured Pt concentrations such that the reported $D_{Pt}^{met/sil}$ will depend highly on the degree of success one has at avoiding nugget-bearing glass. The resultant scatter in the data is therefore attributed to varying degrees of micro-nugget "contamination."

Many studies have therefore concluded that $D_{Pt}^{met/sil}$ is $\geqslant 10^8$, with an "accepted value" of 10^{15} (Walter et al., 2000) by ignoring the Pt nugget "contaminanted" experiments and by extrapolating low pressure–temperature, high f_{O_2}, Fe-free experiments, to core formation conditions (e.g., Borisov and Palme, 1997; Ertel et al., 1999; Fortenfant et al., 2003). Such $D_{HSE}^{met/sil}$ are far too high, and also too dissimilar among the HSE (spanning greater than nine orders of magnitude at low pressure and temperature), to be consistent with metal–silicate equilibrium during core formation.

We find this approach unsatisfying for several reasons: (1) it is unclear whether solution mechanisms of oxidized species, such as Pt^{2+} can be extrapolated $\geqslant$7 orders of magnitude in f_{O_2} to the fugacities appropriate for core formation. At a minimum, such extrapolations ignore lower oxidation states such as Pt^{1+} and Pt^0—even though monovalent states are important species in solution for at least Pd, Au, and potentially Re (e.g., O' Neill et al., 1995; Ertel et al., 2001). (2) The relevance of Fe-free polymerized compositions to core separation from peridotite is doubtful. (3) Discarding enigmatic and/or poorly understood data may result in throwing out the true signal, not noise. The "contamination" hypothesis fails to identify a mechanism by which nuggets form and it cannot easily explain some of the more enigmatic features, such as nuggets with compositions that differ significantly from the metal source phase (Lindstrom and Jones, 1996; Ertel et al., 1999).

We present evidence here for an alternate interpretation. Analysis of new experiments suggests that micro-nuggets

are *not* contamination and are *not* present at high pressure and temperature. Rather, because Pt solubility in silicate is temperature dependent, micro-nuggets form on quench due to the sudden drop in temperature. If micro-nuggets form on quench from the Pt that was in solution at pressure and temperature, then the micro-nuggets should be included in the dissolved metal budget of the liquid silicate under the experimental conditions.

This alternate interpretation has substantial implications for $D_{Pt}^{met/sil}$, and hence core formation.

1.2. HSE partitioning in a magma ocean

Equilibrium conditions in a hot, deep magma ocean appear to account for the MSE mantle signature. Do the equilibrium (or "mean" polybaric/polythermal) conditions that have been proposed to account for the MSE signature also account for the HSE signature? Unfortunately, HSE micro-nuggets cloud interpretation of experiments performed directly on relevant melt compositions at low f_{O_2}, and the temperature and pressure dependencies of HSE partitioning remain largely unresolved variables.

1.2.1. Temperature

Using multiple linear regression, Righter and Drake (1997) predict a negative correlation between T and $D_{Re}^{met/sil}$, such that the mantle abundance of Re may be explained by a magma ocean at high pressure and temperature. However, the effect of temperature on $D_{Re}^{met/sil}$ has never been investigated systematically. Righter and Drake (1997) must therefore make large extrapolations in P, T, X, and f_{O_2} to derive a temperature dependence from disparate data. Moreover, controversy over the nugget-effect led Ertel et al. (2001) to question the inherent value of the solubility data included in the regression in the first place.

Fortenfant et al. (2003) show that Pt solubility in Fe-free silicate increases by a factor of two as temperature is increased over 200 °C (to 1550 °C) at 1 atm and $f_{O_2} = 10^{-2.5}$ (under such oxidizing conditions, micro-nuggets do not develop). They extrapolate their results >1000 °C in temperature and >6 orders of magnitude in f_{O_2} to reach the likely temperature and f_{O_2} of a terrestrial magma ocean. While Fortenfant et al. (2003) conclude that $D_{Pt}^{met/sil}$ does not decrease sufficiently with T to overcome its purported increase with falling f_{O_2}, they only consider the regime where the solution of Pt is as Pt^{2+}. Extrapolations from that regime to very different T, f_{O_2}, and X, warrant caution.

Finally, Danielson et al. (2005) show in a recent abstract that $D_{Au}^{met/sil}$ may fall over two orders of magnitude from those measured at low temperature and 1 atmosphere when conditions approach those of a magma ocean (2000 °C, 27 GPa, low f_{O_2} and high f_{S_2}).

1.2.2. Pressure

While increases in pressure appear to reconcile mantle abundances of the moderately siderophile elements with experiment (Li and Agee, 1996; Righter et al., 1997; Gessmann and Rubie, 1998, 2000; Chabot and Agee, 2003; Chabot et al., 2005), results for Pt and Pd at high pressures have not thus far shown a convincing pressure effect (Holzheid et al., 2000); though again, micro-nuggeting complicated interpretation of the experiments.

To remediate the paucity of HSE partitioning data under relevant conditions and to avoid extrapolations in T, f_{O_2}, and X, the current study investigates the solubility of Pt in reducing mafic melts to temperatures up to 2500 °C at 2.2 GPa.

2. Methods

2.1. Experimental

To execute long-duration, moderate-pressure experiments at temperatures in excess of 2000 °C, we implemented a new cell assembly for the piston cylinder. The 1.25 in. long cell consists of pressed $BaCO_3$ (1/2 in. OD and 3/8 in. ID) wrapped with Pb foil to both lubricate the pressure vessel bore and contain the friable $BaCO_3$ cell during construction. A Ca^{2+} doped $LaCrO_3$ insulator (3/8 in. OD 1/5 in. ID) protects the $BaCO_3$ from the heater. We doped the $LaCrO_3$ with Ca (as opposed to the usual Cu dopant) to prevent reduction of Cu^{2+} to Cu metal by the graphite heater and to enhance the material's radiation damping opacity. To make the insulators, we combined La_2O_3 in equal molar proportions with Cr_2O_3. We added $CaCO_3$ to make 2 wt% Ca. The mixture was shaken, pressed into pellets in a 1 in. die and fired in a Ni crucible in air for 6 h at 1000 °C. Complete reaction was signaled by the color change from bright green to chocolate brown. This powder was then combined in a ratio of ≈11:1 with copy toner to bind it, and pressed to final dimensions in a P.T.F.E. lubricated carbide die to 3000 psi for ≈3 min. After extraction from the die, the insulators were heated on a ramp at 1000 °C/h to 1050 °C, held for 1 h and then allowed to cool in the oven.

We cut the graphite heater (1/5 in. OD, 1/8 in. ID) short to 1 in. length to reduce heat loss to the piston. 1/8 in. long MgO end plugs wrapped in 0.001 in. thick Mo foil completes the heater circuit. A D-type thermocouple ($W_{75}Re_{25}/W_{97}Re_3$) sheathed in 4 bore MgO monitors the temperature. All other spacers are MgO which also insulates the graphite sample container from the graphite heater (Fig. 1). We placed small clippings (0.0001–0.0005 g) of 100% platinum wire (± an equivalent mass of iron metal powder) in the bottom of the graphite capsule. We packed 0.0015–0.0025 g of MAR basalt or MT-7C komatiite (Table 1) in on top.

Our experimental objective is to measure Pt concentrations in a glass free from micro-nugget contamination. We therefore attempt to remove all previously suggested mechanisms of Pt contamination. We reason that if the only means of Pt entry to the glass is via dissolution, and Pt solubility is temperature dependent, then any micro-

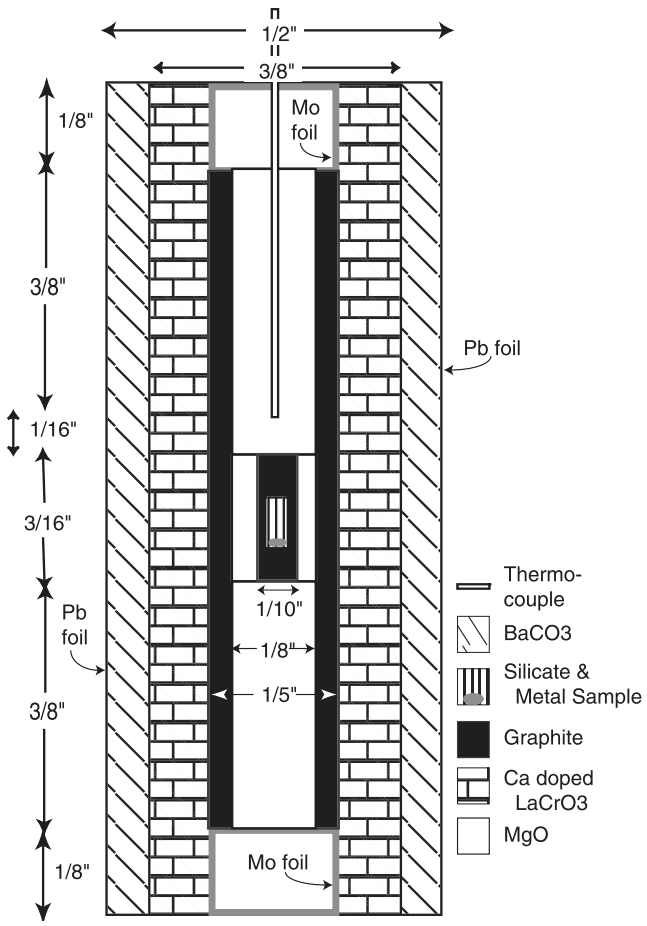

Fig. 1. Piston–cylinder assembly for experiments above 1600 °C.

nuggets found in the quench glass must result from dissolution followed by precipitation upon quench due to the temperature drop. The geometry of the experiment therefore serves three crucial functions, all directed toward suppressing Pt addition to the glass by any means other than dissolution. First, the Pt source begins gravitationally below the initially Pt-free silicate such that no buoyancy-driven mechanical mixing between starting materials can take place before or during run conditions. No parts of the capsule contain Pt nor do we employ Pt stirring spindles, etc. Second, we place the charge in the thermal gradient of the heater such that the top of the charge is about 20 °C hotter than the bottom. This configuration should eliminate thermal convection because if the liquid is hotter on top, it is buoyant. This placement prevents Pt from being "torn up" by a vigorously convecting liquid, a further precaution against mechanical mixing via advection. Finally, we do not use silicate reduced from a previously oxidized (Pt-saturated) condition because it has been argued that micro-nuggets may precipitate out of over-saturated melts and then fail to migrate out of the silicate (O' Neill et al., 1995; Walter et al., 2000). Because our silicate begins with no dissolved Pt, we eliminate this mechanism.

We also considered the possibility that vapor transport between the grains during sintering might redistribute Pt before run conditions. We therefore sintered an experiment for over 4 days and then brought it to 1500 °C just long enough to melt the silicate. No micro-nuggets were present in the quenched silicate glass, suggesting that at 2.2 GPa Pt oxides are not vapor-mobile during sintering.

Only in the reversal experiments were Pt and silicate in intimate contact prior to the run conditions. To approach equilibrium from the direction of Pt over-saturation, we mixed PtO_2 powder with silicate in a 1:10 ratio prior to run conditions. The reversal experiments ensure that our measured $D_{Pt}^{met/sil}$ are equilibrium values and also allow us to investigate the time frame necessary to reach equilibrium. Some low-temperature studies, using Pt crucibles to equilibrate hundreds of grams of material, suggest that hundreds, and perhaps thousands, of hours are necessary to equilibrate silicate and HSE metals (Ertel et al., 1999). Other low temperature wire-loop studies involving small aliquots of silicate also suggest that tens of hours are necessary for equilibration (Borisov and Palme, 1997). Such equilibration times could have far reaching consequences both for experimental work as well as for metal–silicate equilibration during core formation. At high temperature we find that the metal–silicate system reaches stable, but noisy, values quite rapidly, in line with other experimental studies of the siderophile elements in this pressure–temperature regime (e.g., Thibault and Walter, 1995).

We loaded the assemblies into a $\frac{1}{2}$ in. Boyd-England type piston–cylinder apparatus, pressurized them to run pressure using the cold piston-in technique, and sintered them for at least 8 h at 800 °C. We controlled the temperature with a Eurotherm 800 series controller and pressure was kept at 2.2 GPa. Pressure was calibrated for thin walled $BaCO_3$ cells using the known melting point of

Table 1
Experimental silicate starting compositions

Oxide wt%												
Composition:	nbo/T[a]	SiO_2	TiO_2	Al_2O_3	Cr_2O_3	MgO	CaO	MnO	FeO	Na_2O	K_2O	Total
MAR[b]	0.78	49.6	1.23	15.24	—	9.09	11.36	0.18	12.34	2.56	0.09	101.7
KOM[c]	2.00	46.0	0.35	7.61	0.34	25.80	7.45	0.17	10.40	0.51	0.11	98.7

[a] Calculated according to the procedure of Mills (1993).
[b] Mid-Atlantic Ridge Basalt, sample AII-129-6, LDEO-unpublished in-house ICP-MS standard powder (Su, 2002).
[c] MT-7C, from Munro Township in the Abitibi belt of Canada, dehydrated 12 h at 800 °C at the IW buffer. The mixture was fused for 2 h at 2000 °C and 2 GPa in the same assembly as the experiments (but in the absence of Pt). We analyzed the quenched glass with electron microprobe according to the procedures of Section 2.2.2.

Au as a function of pressure [$kbar_{sample} = 0.0959 \cdot (bars_{oil\ in\ a\ 5\ in.\ ram}) - 0.8243$. Kevin Wheeler, pers. comm.]. After sintering, we heated the experiments to reach 1300 °C in 5 min and held them for ~20 min before rapidly heating them (in less than 1 min) to run temperature. The respite at 1300 °C improved the high temperature stability. We quenched the experiments after 1–10 h by shutting off power to the furnace. We sectioned the experiments and double-side polished them for examination in reflected light, transmitted light, and for EMP, SEM, FTIR, Raman, and LA-ICPMS analysis.

At high temperature, pressure vessel exteriors remain lukewarm. Even after 10 h at 2000 °C, neither pistons nor pressure vessels were ever damaged. In the longest and/or hottest runs, thin (100–400 μm) reaction zones of interlaced graphite and $LaCrO_3$ developed at the graphite-insulator interface at the hot spot. We did not observe reaction zones in runs shorter than 3 h and less than 2200 °C.

The new piston cylinder design provides an alternative to the multi anvil for high temperature experiments below ≈3 GPa and has the advantages of larger sample volumes and longer run times in a simple assembly.

2.2. Analytical

2.2.1. Scanning electron microscope

We examined all experiments optically and with scanning electron microscopy. We performed SEM analyses on carbon coated samples on the Lamont-Doherty LEO 1455 VP in high vacuum mode at 25 kV. We imaged the experiments with BSE and collected semiquantitative spectra using energy-dispersive X-ray analyzer EDAX Phoenix Pro with theoretical standards at ≈3000 cps and 35% dead time. Image size varied from sub-micron to 200 μm depending on the size of the desired field of view. We analyzed micro-nuggets using energy dispersive spectra on the SEM with a <1 μm diameter beam. Count times were usually 200–300 s.

2.2.2. Electron microprobe

We performed preliminary EMP analyses on the CAMBAX electron microprobe at Lamont-Doherty Earth Observatory. We then carried out quantitative analyses at the American Museum of Natural History using the CAMECA SX100. We analyzed major elements using a 10 μm beam at 15 kV accelerating voltage and 20 nA sample current (4 nA for Na_2O and K_2O). We used the Phi Rho Z correction scheme. We monitored the silicate composition using Juan de Fuca basalt as a comparison standard.

We performed Pt analyses in trace element mode using both point-mode (~ 2μm) and 20 μm beam diameters. The accelerating voltage and current were 25 kV and 140 nA, respectively. Using the LiF crystal, we counted at the $Pt_{L\alpha}$ peak position for 300 s and at ±600 spectrometer steps off peak for 50–300 s to measure the background correction. (There are 10^5 spectrometer steps between Bragg angle sin Θ of 0 and 1.) We used pure Pt wire as a standard. Under these conditions, the detection limit for Pt in the silicate is ≈30 ppm at the 95% confidence level. Monitoring of Juan de Fuca basalt returned a Pt concentration of 0.0000 wt% quantitatively in all analyses. We also analyzed experiments of identical configuration and composition run at lower temperatures (1400–1600 °C) for the presence of Pt. While analysis of the silicate glass from low temperature runs with LA-ICP-MS (see below) revealed the presence of ≈0.1–1.0 ppm Pt, EMP did not return Pt counts distinguishable from background.

These tests suggest that EMP is sufficiently sensitive to detect tens of ppm Pt reliably. They also confirm that the Pt concentrations we measure with LA-ICP-MS are consistent with values from the literature for glasses equilibrated at low temperature and that these same concentrations lie below the detection limit of EMP as expected.

Metal liquids quenched as dendritic carbon-bearing (≈1–5 wt% carbon) polycrystalline aggregates. We therefore used a defocused 50 μm beam at 25 kV and 40 nA to assess the bulk metal composition at pressure and temperature.

Continuum fluorescence effects present a challenge to EMP analysis of HSE concentrations in experimental systems. The high mass fraction of HSE in alloy compositions and the use of pure HSE metal phases in experiments make EMP analyses highly susceptible to contributions from the metal phase. The light silicate matrix does not efficiently damp continuum X-rays at the high energy needed to excite high atomic number elements, such as Pt. This can result in apparent Pt concentrations of tens to hundreds of ppm above the true concentrations (Cottrell, 2004). In the presence of low Pt concentrations in the glass, any contribution from continuum excitement of spatially adjacent metal phases is an unacceptable analytical artifact.

The magnitude of the effect depends on the Pt metal geometry; therefore, correcting for the effect is impractical. To avoid any complications, we performed all analyses presented in this paper with Pb foil completely covering the entire charge save a silicate "window" or by separating the silicate and metal completely. Pb foil absorbed any Pt X-rays generated by adjacent metal phases excited by continuum fluorescence.

We also doubly polished the charges to allow light transmission, thereby ensuring that Pt metal was not lurking beneath the silicate surface. While tedious, this is the only way in which one can be assured a clean analysis. In general, special care should be taken when using EMP to analyze $D_{HSE}^{met/sil}$.

2.2.3. LA-ICP-MS

We used laser ablation inductively coupled mass spectrometry (LA-ICP-MS) to monitor experimental glasses for the presence of micro-nuggets that could potentially fall below detection by SEM-BSE imaging (Ertel et al., 1999). We performed the analyses on the Lamont-Doherty Earth Observatory PQ2+ ICP-MS with S-option in real-time acquisition mode and in conjunction with a 193 nm

argon–fluorine excimer laser (Lambda Physik). The operating conditions are presented in electronic supplement EA-1. We monitored Pt isotopes 194, 195, and 196 for the appearance of concentration "blips" indicating inhomogeneous distribution of Pt in the glass. NIST glasses 610 (3.15 ppm Pt) and 612 (2.59 ppm Pt) were used as standards (Sylvester and Eggins, 1997).

2.2.4. FTIR

We analyzed the vesicles in the quenched silicate glass of experiments GG090503, GG112003, and 4P092103 for the presence of volatiles using Fourier transform infrared spectrometry (FTIR). Suspecting that the graphite capsule might serve as a source of volatiles, we looked for evidence of dissolved C-species (CO, CO_2). We conducted room-temperature measurements in transmittance mode using a Nicolet 20SXB FTIR spectrometer attached to a Spectra Tech IR Plan microscope at the American Museum of Natural History. Both the IR objective and the spectrometer were purged with dry nitrogen gas at a rate of 15 L/min. We collected transmittance IR spectra over the mid-IR (1400–4000 cm^{-1}) to near-IR regions (6500–3700 cm^{-1}) using a KBr beam splitter, MCT/A detector, and globar source.

2.2.5. Raman

Jill Pasteris analyzed vesicles in experiment 4P092103 for vapor phase contents using the Raman microprobe at Washington University. This fiber-optically coupled microscope-spectrometer-detector system is configured with a 532-nm Nd-YAG visible laser with maximum output of 100 mW, an *f*/1.8 holographic imaging spectrograph, a 2048-channel CCD array detector, and a research-grade Leica polarizing-light microscope that can be used in the transmitted- or reflected-light mode. The samples in this study were analyzed using an 80X ultra-long-working-distance Olympus objective with a numerical aperture of 0.75, which brought 15–16 mW of power onto the surface of the sample. Most spectra represent the accumulation of 20 s of counting time (Jill Pasteris, pers. comm.).

3. Results

All high *T* experiments quenched to a crystal-free glass that remained cleanly segregated from the metal source. The silicate glass displays textural zoning concentric with respect to the margins of capsule–glass interface (Fig. 2). We observed vesicles within the silicate interiors of the charges while the edges adjacent to the graphite capsule are free of vesicles. Pt micro-nuggets (100 nm–1 μm) appear on the interior of the silicate charges along with the vesicles. Micro-nuggets are also found in a band encompassing the vesicle-bearing interior. In contrast, the quenched silicate glass "rim" adjacent to the graphite is free of both vesicles and micro-nuggets (Figs. 2 and 3). The width of the nugget-free zone varies but is typically on the order of 20–50 μm in width. We determined that the rims were nugget-free with SEM in BSE mode at <100 nm resolution and confirmed the absence of Pt nuggeting with LA-ICP-MS; we saw no "spikes" in Pt concentration during real-time acquisition while ablating the glass in these rims. (Ertel et al. (1999) report resolution of nuggets with diameters of ⩽0.05 μm using this technique.) In contrast, Pt-spikes were visible in the central areas with visible PtFe micro-nuggets.

Fig. 2 illustrates an example of this experimental "quench" texture which we believe results from gradients in cooling rate within the silicate volume. Hereafter, we refer to the micro-nugget-free and vesicle-free edge as the "quench margin," reflecting our interpretation.

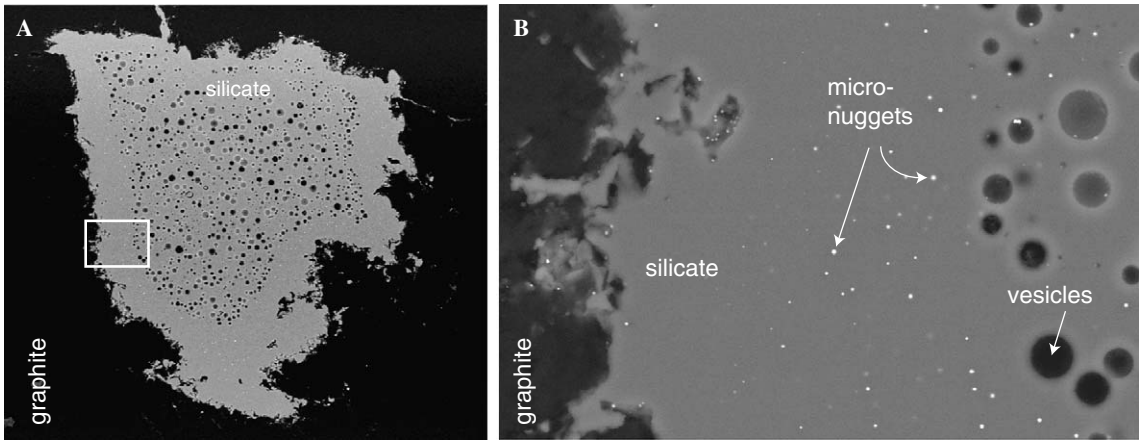

Fig. 2. Quench textures in the silicate. (A) BSE image of experimental charge GG100803 run at 2400 °C. (B) Boxed area in (A). Width of the box is 110 μm. Light gray area is polished silicate glass surrounded by black graphite capsule. Vesicles and micro-nuggets are abundant in the interior. The vesicle + nugget region is ringed by a narrow (≈20 μm) band of silicate containing PtFe alloy micro-nuggets. Outside of this region lies a band of nugget- and vesicle-free silicate, proximal to the graphite-silicate interface, and about 50 μm wide. The absence of both the micro-nuggets and the vesicles therefore depends on spatial proximity to the graphite–silicate interface. This texture, and other textural and compositional evidence presented in the text, supports a quench origin for nuggets and vesicles.

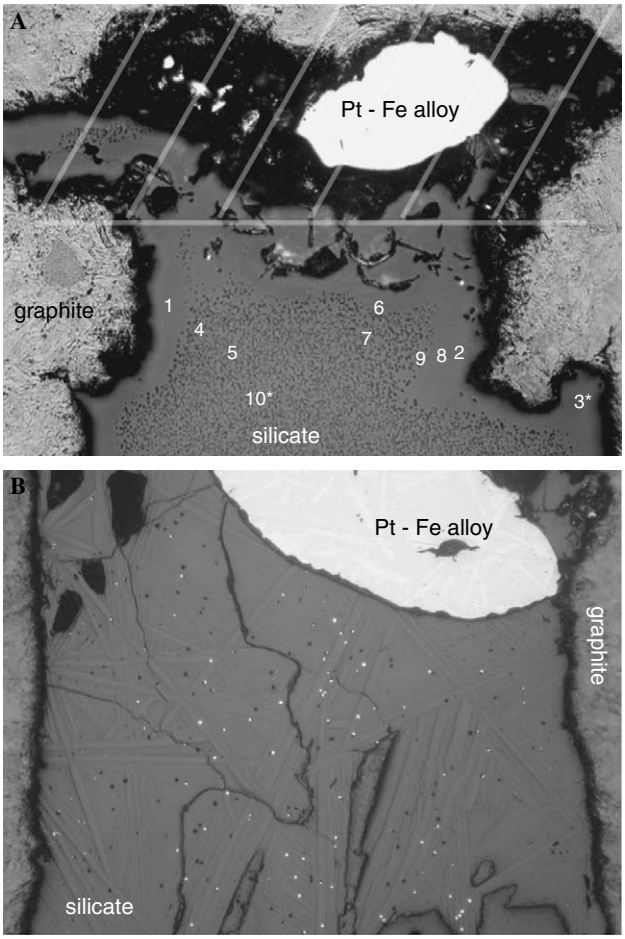

Fig. 3. Photomicrographs of experiments (A) GG112003 (2000 °C, 70 min) with reference to Table 2 and (B) GG111303 (2500 °C, 21 min) taken in reflected light show Pt distribution in the silicate. The width of each photo is 0.75 mm. Both images show clear textural zoning relative to the silicate–graphite interface, implying that edges in contact with graphite and metal cooled more rapidly than the silicate center. Edges are free of micro-nuggets and vesicles. Micro-nugget diameter appears to be controlled by quench rate, not run time. Frame (A) quenched very rapidly without development of any micro-nuggets on optical or BSE imaging scales (down to 100 nm) in the vesicle free "chill margin." Vesicles are ≈2 μm across. Measured Pt concentrations for numbered points are in Table 2. White diagonal lines indicate the area that was covered with Pb foil during analysis. Frame (B) quenched more slowly (from 2500 to 800 °C in ≈10 s), allowing a spinifex + nugget texture to develop. Runs as long as 10 h at 2000 °C show no increase in micro-nugget size as might be expected from a dissolution–reprecipitation mechanism or Ostwald ripening acting during the 1–10 h duration of the experiment.

We postulate that a smelting reaction produces the vesicles on quench. During the high pressure and temperature phase of the experiment, the graphite capsule enforces a low f_{O_2} as evidenced by the low FeO contents of the silicate phase and the formation of the FePt–liquid–alloy metal phase. (In some experiments we kept FeO abundant in the silicate phase through the addition of Fe metal to the charge.) In all experiments some FeO remained in the silicate. We postulate that this FeO was reduced to form the Fe–Pt nuggets and CO vesicles when temperature and pressure were lost on quench via the smelting reaction $C + FeO \rightarrow Fe_{metal} + CO/CO_2$.

There is no evidence that the vesicles exist at run conditions. First, it is difficult to imagine the existence of any free gas phase in this system at 2.2 GPa. Second, the bubbles neither rise nor coalesce nor exist within the quench margin, further supporting the theory that they form on quench.

We calculate that only tens to thousands of bars of CO partial pressure could have existed under the high pressure and temperature run conditions. This calculation uses the Fe–FeO equilibrium between metal and silicate phases measured after quench to estimate a_{Fe} and a_{FeO} according to the formulation of Hillgren et al. (1994) (see our treatment of f_{O_2} below). We used these activities to derive f_{CO} based on the following equilibria:

$$C + \tfrac{1}{2}O_2 = CO \quad (2)$$

$$Fe + \tfrac{1}{2}O_2 = FeO \quad (3)$$

Subtraction of Eq. (3) from (2) yields the smelting reaction

$$C + FeO = Fe + CO \quad (4)$$

The equilibrium constant for this reaction, κ_4, at carbon saturation ($a_C = 1$) is

$$\kappa_4 = \frac{\kappa_2}{\kappa_3} = \frac{a_{Fe} \cdot f_{CO}}{a_{FeO}}. \quad (5)$$

We derived κ_2 and κ_3 from thermochemical tables over a range of experimental T and f_{O_2} (2000–2500 °C and $\Delta IW \sim -1$ to -5) and at total sample pressure $P_{total} =$ 22,000 bars to arrive at $f_{CO} =$ 50–4000 bars under run conditions (Chase, 1998).

These CO partial pressures cannot have supported open vesicles at 20,000 bars of total sample pressure at P and T or at 15,000 bars of assembly pressure consistent with the ram oil pressure remaining after thermal quench. The pressure discrepancy between the quench pressure on the melt (inferred from the presence of CO-filled vesicles) and the recorded sample load pressure indicates that the high temperature design itself may prohibit concordance between the load pressure and the true sample pressure immediately following quench. Because sintered $LaCrO_3$ becomes mechanically strong after prolonged periods at high pressure and temperature, it is possible that the $LaCrO_3$ cylinder is "holding open" the inner cavity after quench, allowing the silicate pressure to drop radically while causing the load gauge to record ≈15,000 bars. We calculate an expected 100,000–200,000 bar thermal pressure drop for a drop in temperature of 2000 °C for the pressure media (MgO and graphite) in a rigid container—more than adequate to explain the discrepancy we record between CO vapor pressure and sample pressure. Alternative explanations (such as the pressure calibration being off by three orders of magnitude or friction in the bore) seem unlikely.

FTIR analyses did not detect carbon bearing species in any significant abundance in the bulk glass, though they must have been present because Raman analyses revealed the presence of CO in abundance within individual vesicles.

Spectra taken with 1 μm spatial resolution on targeted vesicles show a distinct narrow band at about 2140 cm^{-1} for CO, as well as broad bands at about 623, 1230, and 1600 cm^{-1}. This finding supports the textural interpretation given above.

The direct measurement of CO in sealed quench vesicles surprised us. CO species have never been detected in quenched silicate glasses, which has led several investigators to call the existence of this species into question (Dixon et al., 1988; Stolper and Holloway, 1988). CO may dissolve in the melt under run conditions but cannot be "quenched in" (and has thus eluded detection). Alternatively some intermediary species, such as a metal–carbonyl (M–C=O), may be present in the melt at P and T and dissociates upon quench to yield CO + M, however other experimental evidence argues against this second hypothesis (Borisov and Palme, 1997; Ertel et al., 1999). Finally, neutral carbon may dissolve in the melt at run conditions and reduce dissolved iron and platinum on quench to produce the nuggets and vesicles. In all cases the overall reaction is the same [C + MO → CO + M]. If indeed experimental Pt redistribution and solubility are carbon-mediated, the experiments may have special relevance for the Earth's mantle which may be carbon-saturated itself. However, the micro-nuggeting phenomena has been observed in noble metal–silicate partitioning experiments using all manner of technique: wire loop (Borisov and Palme, 1997), stirred crucible (Ertel et al., 1999), as well as other piston–cylinder and multi-anvil experiments in the absence of carbon (Holzheid et al., 2000). This strongly suggests that the presence of graphite is not at the heart of the micro-nuggeting phenomenon.

3.1. Pt distribution in the silicate and evidence for the quench origin of micro-nuggets

Several features of micro-nugget distribution suggest precipitation upon quench. First, micro-nuggets do not coarsen with run time. Experiments at 2000 °C were run from 1 to 10 h with no sign of the nugget growth that might be expected if the micro-nuggets were due to dissolution and reprecipitation during the high pressure and temperature phase of the experiment. Quite to the contrary, nugget diameter appears to be uniquely controlled by the quench rate with slower quenching runs holding the largest nuggets in the central regions of the silicate. Fig. 3 compares two experiments, one of which quenched rapidly, producing a clean glass quench margin around a nugget and vesicle-bearing interior (maximum nugget and vesicle diameters equal to 200 nm and 2 μm, respectively), and one which quenched more slowly, allowing a spinifex + nugget texture to develop through the charge. Nugget diameter decreases toward the quench margins, which are nugget free.

Second, Ertel et al. (1999) and Lindstrom and Jones (1996) show that nuggets have a different composition than the bulk metal source. We confirmed this observation through semi-quantitative spectral analysis of dozens of micro-nuggets per experiment using the energy-dispersive X-ray analyzer EDAX Phoenix Pro on Lamont's SEM. Our qualitative observations (limited by the small and variable size of the nuggets relative to the SEM beam) indicate that experimental micro-nuggets are typically far more iron-rich (factor of 2–10) than the bulk metal phase. This observation does not conclusively point toward a quench origin, however it does favor one.

If Pt and Fe are in solution in the silicate phase at pressure and temperature, and then precipitate as nuggets upon quench, they too should have the same composition as the metal phase in equilibrium with that silicate. In this scenario, however, nuggets might form with a different composition because the elements that compose them have differing diffusion rates. Our experiments require diffusivities as rapid as 10^{-4}–10^{-5} $cm^2\ s^{-1}$. The Pt solubilities we measure at $f_{O_2} < 10^{-5}$ atm have no f_{O_2} dependence (Fig. 4) consistent with all previous studies of HSE solubility under reducing conditions (e.g., Borisov and Palme, 1995, 1997; O' Neill et al., 1995; Ertel et al., 1999; Holzheid et al., 2000) and with neutral Pt speciation. Pt diffusivity may not be constrained by normal expectations for cations if neutrally speciated. For instance, Lux (1987) has reported a diffusivity for neutral Ne of $\sim 3 \times 10^{-5}$ $cm^2\ s^{-1}$ in basaltic liquid at a temperature 100 °C below ours. Ne has a larger effective atomic size (1.6 Å) than neutral Pt (1.4 Å) so, by the precedent of Ne, Pt diffusivities could easily be considerably faster than the minimum values needed to rationalize our observations. Furthermore, if nuggets form over a range of quench temperatures that differ from the equilibrium temperature, the nuggets could differ in composition from the bulk metal phase due to temperature sensitive partitioning effects. In addition, interfacial effects could play a role at these very small scales during precipitation from solution upon quench.

The third and most important observation in support of a quench origin for the micro-nuggets is that Pt concentration does *not* vary spatially within the silicate. As we illustrate in Fig. 3 and Table 2, Pt concentrations are the same in the nugget free quench margins and nugget bearing interiors. The nuggets are so finely dispersed within the silicate interior that most analyses excited Pt-bearing nuggets within the primary excitation volume of the beam. Measured Pt contents in the interior of the silicate have the same range of values as the nugget-free quench margin *because* nuggets were included in analysis of the interior points. This is consistent with a fast quench on the edge, leaving Pt dissolved in the silicate matrix, and a slower quench on the interior which would precipitate Pt out of the matrix and into nuggets. We expect and observe the corollary that measured Pt concentrations are more uniform on silicate edges than interiors (Table 2).

The observation that Pt concentrations in the silicate are the same in adjacent nugget-bearing and nugget free regions is remarkable and unexpected. It implies that Pt is homogeneously distributed at run conditions and the presence/

absence of nuggets is controlled solely by quench rate. If we accept the hypothesis that Pt in the quench nuggets is in solution in the liquid silicate at pressure and temperature, we must shift the focus to assessment of the true average Pt concentration at pressure and temperature for each experiment in order to calculate $D_{Pt}^{met/sil}$. We therefore present a quantitative analysis of sample heterogeneity for each experiment and its impact on reported average Pt concentrations.

Table 3 summarizes the experimental conditions and resultant Pt concentrations in the silicate liquid which range from 24 to nearly 1100 ppm. As discussed above, Pt is heterogeneously distributed in the quenched glass on the micro-scale (<tens of microns), but homogeneously distributed at the macro-scale (>tens of microns). It is therefore instructive to quantify the extent of heterogeneity in the glass. Table 3 reports the percent relative standard deviation (ϵ) of the analyses. ϵ can be considered a measure of the range of concentrations encountered by a random spatial distribution of point analyses on the quenched silicate. For example, Fig. 3 contrasts rapid quench experiment GG112003 with a slow quench experiment GG101303 and illustrates their differing quench textures (very tiny and rather large micro-nuggets, respectively). The percent relative standard deviation is therefore much smaller for the former than the latter as expected.

We also quantify the uncertainty in any given experimental average (which will be proportional to the sample heterogeneity and inversely proportional to the square root of the number of analyses taken). We report this as the standard error of the mean, σ_M, in Table 3; it gauges the confidence we have that the reported average $D_{Pt}^{met/sil}$ is the true average for any given experiment.

Finally, some analytical uncertainty results from the low Pt concentrations. This is reported in Table 3 as σ_C and is the percent relative standard deviation of the average Pt concentration that derives from analytical uncertainty alone. We calculated σ_C by propagating the error in the counting statistics for each individual analysis into the total error on the average. Unsurprisingly, σ_C varies with the overall concentration level. For very low concentrations, σ_C may account for a large portion of the total error associated with an average whereas, when the concentration of Pt is high, σ_C may only carry an insignificant portion of the total uncertainty.

In experiment GG112003, for example, the measured Pt concentration varies by ±64%—including both nugget-bearing and nugget-free regions (Fig. 3A and Table 2). This range is greater than the expected error due to analytical uncertainty ($\sigma_C = \pm 5\%$). A detailed look reveals that heterogeneity does exist on the micro-scale (<tens of microns) due to any individual analysis incorporating greater or fewer nuggets in the interior region of the charge. The measured Pt concentrations in the nugget-bearing regions of sample GG112003 range from 110 to 560 ppm and vary by 71%. In contrast, Pt concentrations in the nugget-free quench margin vary within analytical uncertainty. The average Pt concentrations for the two spatial sub-samples, however, are statistically the same (especially when given the large variability within the nugget-bearing region). Variable quench rates (fastest at the silicate–graphite edge) produces homogeneity on the micro-scale within the quench margin and heterogeneity on the micro-scale on the charge interior. At the same time, the equilibrated silicate at run conditions produces homogeneous Pt distribution on the macro-scale of the sample and the presence or absence of Pt nuggets is immaterial.

This detailed characterization of Pt distribution within the quenched silicate glass underscores our conclusion that Pt concentration in the silicate is not controlled by the presence/absence of micro-nuggets. Rather, the micro-nuggets are a textural feature produced on quench.

We reproduced this quench texture even when the experiments approached equilibrium from an initial condition of excess Pt in the silicate. In our two reversal experiments, GG010705-R and 3P030805-R, in which we physically mixed PtO_2 oxide powder with silicate powder in advance of loading the graphite capsules, Pt was reduced and was excluded from the silicate. The Pt ultimately coalesced as a single mass of PtFe alloy save for the ubiquitous concentric nugget-free and nugget-bearing quench zones. (In contrast, Pt was absorbed by the silicate in the "forward" experiments described above.) Both sets of experiments converged upon the same textures and Pt concentrations and indicate that our values for $D_{Pt}^{met/sil}$ are equilibrium values.

In their discussion of the approach to thermodynamic equilibrium and equilibration timescales, O' Neill et al. (1995) and Walter et al. (2000) suggest that slow Stokes settling velocities of Pt micro-nuggets might limit the migration of nuggets back to the metal source phase following f_{O_2} reduction. This mechanism cannot be active in our forward approach to equilibrium because our glass is not reduced from an oxidized Pt-saturated condition—the glass is initially Pt-free and the reducing conditions are imposed immediately. Because the reversal experiments create an identical texture and composition to the forward experiments (within the overall scatter of this study) we believe that the nuggets in both the forward and reversal experiments formed on quench and that the Pt concentration of the glass reflects the concentration in thermodynamic equilibrium with the metal alloy.

The rapid approach to equilibrium we observe experimentally at these high temperatures comes as no surprise, reaffirming previous experimental experience. A time series by Fortenfant et al. (2003) in An-Di eutectic melt at $\log f_{O_2} = -2.5$ shows a slow approach to equilibrium at low temperature, taking 168 h at 1350 °C. Ertel et al. (1999) made a similar observation at 1300 °C under reducing conditions. Several factors may account for the difference in equilibration times between those studies and the present study: (1) volatilization may have continually changed the melt composition over the two or three weeks in a gas mixing furnace (Borisov and Palme, 1997). (2) Quantities equilibrated in those studies (100 g) are five orders of magnitude larger than those equilibrated in the present

study (1–3 mg). (3) Temperatures were ≈1000 °C lower in those studies. (4) Viscosities in the haplobasaltic melts used in those studies are much higher than those of the basaltic and komatiitic melts used in the present study. (4) The speciation of Pt, and hence the diffusivity of Pt, should differ between those oxidizing studies and the present study at low f_{O_2}. Pt^0 and Pt^{1+} should be fast diffusing species if present in the melt.

Regardless, in our experiments—as in a hot magma ocean—viscosities will be low, diffusivities high, and equilibration between metal and silicate rapid and almost unavoidable (Rubie et al., 2003).

4. Comparison with previous studies

4.1. Oxygen fugacity

We calculated f_{O_2} relative to the iron–wüstite buffer according to Hillgren et al. (1994):

$$\Delta IW = 2\log\frac{X_{FeO}^{silicate}\cdot\gamma_{FeO}}{X_{Fe}^{metal}\cdot\gamma_{Fe}}. \quad (6)$$

We correct for non-ideality in the PtFe metal alloy and silicate using the activity relationships of Hultgren et al. (1971) and Holzheid et al. (1997), respectively.

We present our results as a function of oxygen fugacity using two scales: first, an absolute scale ($-\log f_{O_2}$) without regard for the specific pressure of the experiment, and second, one relative to the Fe–FeO buffer (ΔIW) at the temperature and pressure conditions of the experiment. The absolute scale (Fig. 4A) allows ready comparison among the one atmosphere gas-mixing experiments performed at known, controlled f_{O_2}. Experiments performed under solid-media pressure, however, are more difficult to place on Fig. 4A because their f_{O_2} must be inferred in a less direct manner. Absolute oxygen fugacity must be calculated in two steps, first according to formalism (6) and then by comparison with the position of the iron–wüstite (IW) buffer at the pressure–temperature conditions of the experiment. The activity of oxygen at very high pressures is poorly known; we therefore calculate the IW buffer at experimental temperatures according to the T–f_{O_2} relationship of Huebner (1972) without correction for pressure. This procedure would produce a satisfactory metric for cross-comparison between the experiments if there was little relative shift between the various buffer curves in T–f_{O_2} with pressure. Because such a proposition is unlikely, Fig. 4B uses formalism (6) to locate the high pressure experiments with respect to IW. The 1 atmosphere experiments can be located unambiguously with respect to IW at their experimental temperatures because the location of IW at one atmosphere with respect to temperature is well known experimentally to about 1000 K, and well beyond in temperature by reasonable extrapolation. To the extent that the activity coefficients in Eq. (6) are accurate, Fig. 4B offers the more rigorous arena for comparison of the experiments. We use Fig. 4B to compare redox of the experimental suites and the redox conditions during core formation. Based on the ratio of X_{FeO}^{mantle} to X_{Fe}^{core}, core formation took place at 2–2.5 log units below the IW buffer. In order to represent this f_{O_2} condition in Fig. 4A, one must constrain (or presume) the temperature during core formation independently, whereas Fig. 4B allows direct comparison of the experimental data and core formation redox.

Fig. 4A is useful, however, because it highlights the well-characterized dependence of Pt solubility on f_{O_2} under oxidizing conditions. Fig. 4A also reveals the effect of extrapolating the high f_{O_2} data down to low f_{O_2} while holding the slope constant. This practice of extrapolation does not allow for low valance speciation or changes in solubility mechanism at low f_{O_2}; it therefore predicts sub ppt Pt solubilities during core formation, and correspondingly high $D_{Pt}^{met/sil}$.

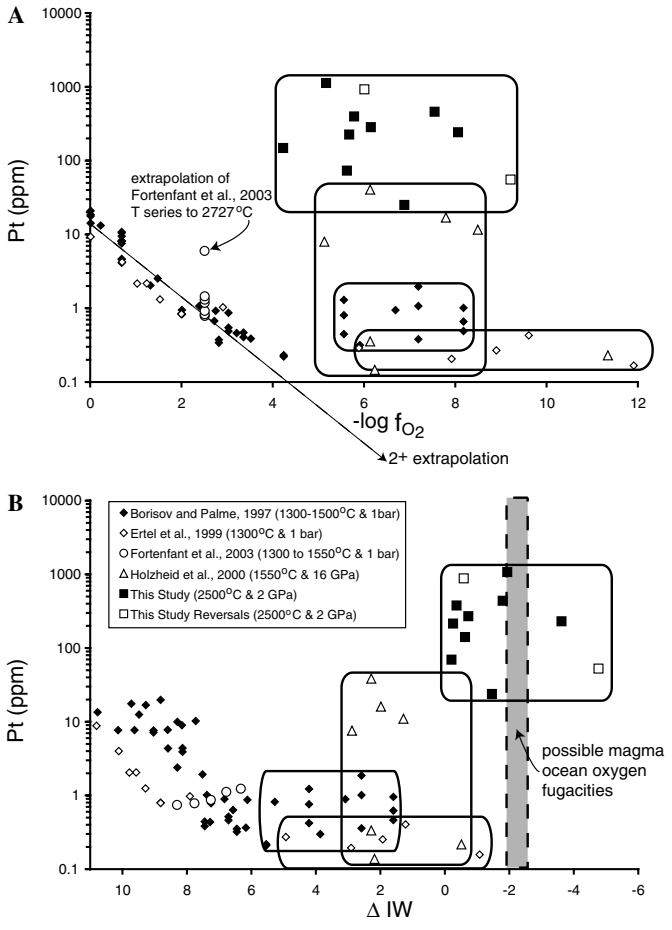

Fig. 4. Pt concentrations in silicate liquids saturated with Pt metal or a Pt-rich Fe alloy compared as a function of (A) absolute f_{O_2} and (B) relative f_{O_2} (ΔIW = 0 = the iron–wüstite buffer). T ranged from 1300–1600 °C in all studies except the present study (2000–2500 °C). Fe-free compositions (An–Di eutectic) were used in one bar studies. The study by Holzheid et al. (2000) used a low melting KNSF silicate while the present study used basalt and komatiite starting compositions. Shaded field represents f_{O_2} appropriate for the early Earth.

Table 2
Pt concentrations in experiment GG112003 corresponding to numbered points in Fig. 3A

	Nugget-free			Nugget-bearing band and interior							Overall
Point No.:[a]	1	2	3[b]	4	5	6	7	8	9	10[b]	$\bar{X}$[c]
Pt (ppm):	170	170	190	150	110	330	220	120	130	560	215
$\bar{x}$[d]		176						231			215
σ_M[e]		6.7						62			43
ϵ (%)[f]		6.5						71			64

[a] Analyses correspond spatially to numbered points in Fig. 3A.
[b] Position approximate—analysis from other side of doubly polished thin section.
[c] Sample mean.
[d] Mean of the spatial sub-sample.
[e] Standard error of the mean ($\sigma_M = \sigma/\sqrt{n}$, where σ = standard deviation and n = number of points).
[f] Percent relative standard deviation ($\epsilon = \frac{\sigma}{\bar{x}} \cdot 100$).

If the nuggets are seen as contamination and divalent Pt is the only species assumed, a decrease of one order of magnitude in solubility is applied for every two orders of magnitude decrease in f_{O_2}. In other studies this requires extrapolation in f_{O_2} of $\geqslant 7$ orders of magnitude (Borisov and Palme, 1997; Ertel et al., 1999; Fortenfant et al., 2003) to 4 orders of magnitude (Holzheid et al., 2000). In stark contrast, if the nuggets are assumed to represent the solubility at pressure and temperature and monovalent and neutral species are considered, then the low f_{O_2} solubilities have a very different functional form, becoming f_{O_2}-invariant at low f_{O_2} (Fig. 4 and Section 3.1). This latter interpretation requires no extrapolation in f_{O_2}.

The practice of ignoring the analysis of experiments performed at low f_{O_2}, and extrapolating Pt solubilities determined at high f_{O_2} to $f_{O_2} <$ IW, influences the calculated $D_{Pt}^{met/sil}$ during core formation more than any other factor. The magnitude of the effect dwarfs any reported dependence on pressure, temperature, metal composition (given that all experiments were performed using Pt or Pt dominated alloys), or silicate composition.

4.2. Pressure, temperature, and composition

Our experiments strongly indicate that nuggets form on quench and were in solution during run conditions. Assuming for the moment that nuggets in all experiments formed on quench, and setting aside small differences in X_{metal}, direct comparison of the Pt concentrations in silicate glass measured *below* $\Delta IW + 6$ reveals the effects of temperature and composition (Fig. 5). Extrapolation of the high f_{O_2} temperature series predicts an increase in Pt solubility of one order of magnitude for a 1500 °C increase in temperature (Fortenfant et al., 2003). Comparison between the various low temperature studies (1300–1600 °C) and this study (2000–2500 °C) confirms a large temperature effect, and suggests an even larger one than extrapolation of the low temperature experiments predicts (Fig. 5). But the effect of increasing temperature is not known, nor necessarily expected, to be linear. Temperature increases change the silicate melt structure. In the limit, high temperatures can lead to closure of the metal–silicate phase solvus such that partition coefficients may converge to unity at the highest temperatures (Murthy, 1991; Walker et al., 1993).

Holzheid et al. (2000) concluded that P does not serve to increase Pt solubility in any systematic fashion between 1 and 16 GPa. Yet, Holzheid et al. (2000) measure over 10 ppm Pt in 4 out of 6 experiments—higher Pt concentrations than any of the 1 bar iron-free experiments—under conditions equally reducing and at similar temperatures to the 1 bar studies. It may be that most of the pressure effect occurs in the first few GPa, as Kegler et al. (2004, 2005) demonstrate for $D_{Ni}^{met/sil}$ and $D_{Co}^{met/sil}$. This is not so surprising if one considers that the difference in pressure between 1 atmosphere and 1 GPa spans four orders of magnitude while that between 1 and 10 GPa spans one order of magnitude. Still, noise in the Pt concentrations measured below $\Delta IW + 6$ within each study covers one to two orders of magnitude, diminishing the illumination of any meaningful pressure dependence that may exist.

Composition varies significantly among the studies compared in Figs. 4 and 5. The natural basalt employed in the current study, the alkali silicate used by Holzheid et al. (2000) ('KNSF' (wt%) = 64.3 SiO_2, 18.6 K_2O, 12.4 Na_2O, and 4.6 FeO), and the An-Di eutectic composition used in the low pressure and temperature studies, have similar nbo/T ratios, revealing no simple relationship between nbo/T and Pt solubility. However, nbo/T provides only one parameterization of melt structure and does not capture stereochemistry effects. The structural consequences of depolymerization with alkali versus alkali-earth elements differ. Moreover, nbo/T does not characterize the specific role that iron may play.

In summary, while the specific consequences of using a low melting alkali silicate or an iron-free silicate versus a natural basalt or komatiite are difficult to quantify, we reason that the most direct means of assessing $D_{Pt}^{met/sil}$ during core formation requires experimentation on relevant geological compositions at relevant T and f_{O_2}.

4.3. Implications for $D_{Pt}^{met/sil}$

Application of experimental partitioning data to metal silicate differentiation in a magma ocean must take into ac-

Table 3
Experimental conditions and results

Press:	GG	4P	GG	GG	GG	GG	GG	GG	4P	GG	3P
ID:	090503	092103	100803	101303	111303	112003	112403	010604	010604	010705-R[a]	030805-R[a]
Silicate[b]	MAR	MAR	MAR	MAR	KOM	KOM	MAR	KOM	KOM	MAR	MAR
Time (min)	67	600	60	540	21	70	60	180	20	233	30
T (°C)	1940	2000	2400	2000	2500	2000	2200	2000	2000	2000	2200
P (GPa)	2.3	2.3	2.2	2.2	2.3	2.2	2.2	2.2	2.2	2.2	2.2
ΔIW[c]	−2.34	−1.28	−1.17	−0.75	−2.49	−0.80	−4.17	−0.91	−2.01	−1.13	−5.32
Pt concentration in the silicate (ppm) and spatial distribution in the silicate											
Pt (ppm)	440	272	142	70	1078	215	232	380	24	885	53
n[d]	2	13	11	5	4	10	6	9	5	9	9
ϵ (%)[e]	3	63	125	34	136	64	57	131	105	79	39
σ_M[f]	10	48	53	10	731	43	54	166	11	232	7
σ_C (%)[g]	20	12	26	24	2	5	7	4	64	2	29
Silicate analyses (cation wt%)											
Si	26.4	25.83	25.0	22.6	20.6	25.3	25.5	21.2	21.7	22.0	20.9
Ti	0.86	0.81	0.87	0.75	0.01	0.25	0.82	0.21	0.20	0.77	0.84
Al	8.49	8.76	8.68	9.70	5.13	4.67	8.34	3.87	3.88	8.03	8.93
Cr	0.23	0.11	0.81	0.68	0.03	0.17	0.15	0.10	0.15	n.a.	n.a.
Mg	5.71	6.86	6.84	9.30	22.51	17.26	6.98	15.07	16.74	5.98	7.03
Ca	9.05	10.42	10.10	12.01	7.26	5.65	10.79	5.59	4.94	9.84	13.78
Mn	0.17	0.09	0.09	0.00	0.00	0.12	0.11	0.12	0.13	0.11	0.08
Fe	2.65	0.42	0.91	0.15	0.05	0.68	0.63	7.31	8.74	0.99	0.12
Na	1.88	1.23	1.60	0.89	0.13	0.40	0.59	0.32	0.36	1.60	0.20
K	0.07	0.09	0.07	0.05	0.03	0.10	0.04	0.08	0.08	0.13	0.00
O	46.08	46.07	45.62	45.62	45.04	46.22	45.41	41.36	43.24	49.28	50.67
Tot	101.6	100.7	100.6	101.8	100.8	100.8	99.4	95.3	100.2	98.7	102.6
nbo/T[h]	0.64	0.68	0.72	0.92	2.26	1.51	0.72	1.90	2.03	0.73	0.88
Metal analyses in wt%											
Fe metal	36.0	15.0	17.0	7.0	12.4	15.0	55.0	27.0	64.0	17.5	44.6
Pt metal	65.0	83.0	82.0	85.0	81.6	85.8	39.7	72.0	37.0	81.8	55.4
Tot	101.0	98.0	99.0	92.0	94.0	100.7	94.7	99.0	101.0	99.3	100.0
Calculated partition coefficients at run conditions and for infinite dilution in Fe metal											
$\log D_{Pt}^{met/sil}$[i]	3.17	3.48	3.76	4.15	2.88	3.60	3.23	3.28	4.19	2.97	4.02
$\log D_{Pt}^{met/sil}$*[j,k]	$4.05^{0.01}_{0.01}$	$5.70^{0.07}_{0.08}$	$5.81^{0.14}_{0.20}$	$6.62^{0.04}_{0.04}$	$4.96^{0.22}_{0.49}$	$5.81^{0.07}_{0.08}$	$3.35^{0.09}_{0.20}$	$4.45^{0.16}_{0.25}$	$4.95^{0.16}_{0.25}$	$5.16^{0.10}_{0.13}$	$4.48^{0.02}_{0.02}$

[a] Reversal experiment: Pt was added as PtO_2 (Pt source was Pt metal in all other experiments).
[b] Information about starting compositions can be found in Table 1.
[c] Calculated at run conditions: $\Delta IW = 2\log\frac{X_{FeO}^{silicate}\cdot\gamma_{FeO}}{X_{Fe}^{metal}\cdot\gamma_{Fe}}$.
[d] Number of analyses.
[e] Percent relative standard deviation ($\epsilon = \frac{\sigma}{\bar{x}}\cdot 100$, where σ = standard deviation and $\bar{x}$ = sample mean).
[f] Standard error of the mean ($\sigma_M = \frac{\sigma}{\sqrt{n}}$).
[g] Percent relative standard deviation due to counting error alone (i.e. propagation of the counting error (equal to $\sqrt{C^{peak}+C^{bkg}}$) associated with individual analyses into the total error associated with the average for an experiment).
[h] calculated according to Mills (1993).
[i] At run conditions. $D_{Pt}^{met/sil} = \frac{X_{Pt}^{metal}}{X_{Pt}^{silicate}}$.
[j] At infinite dilution in Fe metal (Fig. 6). See text and Eq. (7).
[k] Superscript and subscript report the positive and negative range, respectively, of the partition coefficient associated with σ_M.

count the T, P, f_{O_2}, $X_{silicate}$, X_{metal} of a magma ocean, and the activity–composition relationship for Pt at infinite dilution in Fe metal. In our experiments, the intensive parameters of T, f_{O_2}, and $X_{silicate}$ mimic those in a magma ocean and so require no further extrapolation. As discussed above, pressure seems to have no systematic effect on $D_{Pt}^{met/sil}$. If pressure does play a role, the present study at 2.2 GPa—four orders of magnitude higher in pressure than one atmosphere experiments and within an order of magnitude of magma ocean pressures—should capture most of the variance. If the experimental f_{O_2} conditions are grossly dissimilar to those during core formation, extrapolation of those data to low f_{O_2} conditions must rely on knowledge of the functional form of Pt solubility with changing f_{O_2}. If we have achieved our goal of approximating the P, T, $X_{silicate}$, and f_{O_2} of a magma ocean, we do not need to make any assumptions about Pt speciation in the silicate melt. The experimental redox conditions of our experiments mimic those postulated for a magma ocean based on the FeO content of the modern mantle.

This leaves us to extrapolate from the Pt-dominated metal alloys used in our experiments to FeNi alloys con-

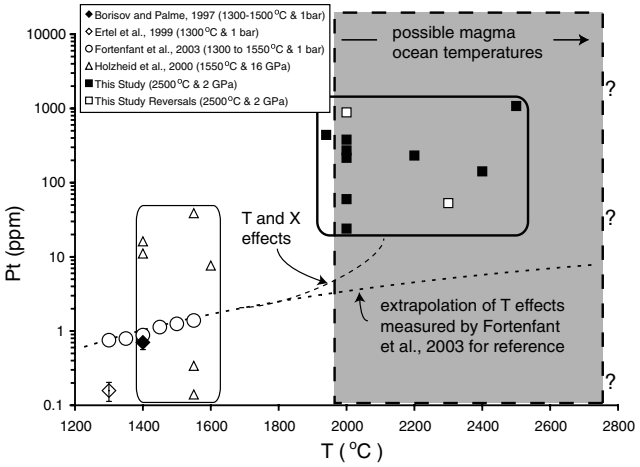

Fig. 5. Experimental data compared as a function of temperature for experiments *below* $\Delta IW + 6$ (with the exception of data from Fortenfant et al. (2003) that is shown to illustrate the magnitude of the temperature dependence measured in that study). Fe-free An-Di eutectic compositions were used in one bar studies. The study by Holzheid et al. (2000), used a low melting KNSF silicate (see text) while the present study used komatiite and basalt starting compositions. Shaded field represents T appropriate for a magma ocean. Symbols as in Fig. 4.

taining only a few ppm Pt expected for the Earth. To derive a Pt partition coefficient relevant to core formation, we therefore calculate $D_{Pt}^{met/sil}*$ according to

$$D_{Pt}^{met/sil}* = \frac{1}{X_{Pt} \cdot \gamma_{Pt}^{Fe,\infty} \cdot A}, \quad (7)$$

where X_{Pt} is the solubility by weight of Pt in silicate in equilibrium with pure Pt metal, $\gamma_{Pt}^{Fe,\infty}$ is the activity coefficient of Pt in iron liquid as $X_{Pt} \to 0$ at the experimental T, and A converts from mole to weight (Borisov et al., 1994). The temperature dependence of $\gamma_{Pt}^{Fe,\infty}$ was extrapolated from binary solution data from Hultgren et al. (1971). The choice of $\gamma_{Pt}^{Fe,\infty}$ can manipulate $D_{Pt}^{met/sil}*$ *at least* three orders of magnitude (for example, see Gudmundsson and Holloway, 1993 versus Hultgren et al., 1971). The uncertainty of $\gamma_{Pt}^{Fe,\infty}$ at the experimental temperatures causes corresponding uncertainty in the conversion of $D_{Pt}^{met/sil}$ measured under experimental conditions to $D_{Pt}^{met/sil}*$.

$D_{Pt}^{met/sil}$ (experimental conditions) at temperatures, silicate melt composition, and f_{O_2} appropriate for a magma ocean yields partition coefficients of 10^3–10^4. At infinite Pt dilution in liquid Fe, we estimate that $D_{Pt}^{met/sil}*$ may be 10^4–10^6.

Fig. 6 presents $\log D_{Pt}^{met/sil}*$ as a function of T for this and other studies from the literature. In this figure, we plot the partition coefficients as they are reported in the literature—with intensive parameters, activity–composition relationships, and Pt speciation in the melt assessed by the authors of each study. Unlike gas-mixing experiments, f_{O_2} and T are not independently controlled in our experiments. We do not normalize our partition coefficients to a fixed f_{O_2} because we believe that extrapolation along f_{O_2} buffer curves

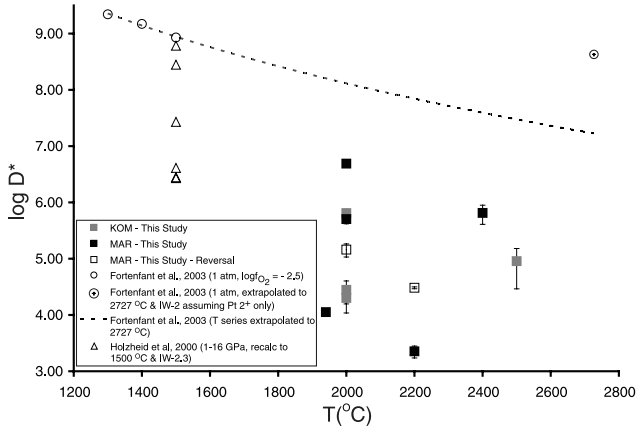

Fig. 6. Dependence of $D_{Pt}^{met/sil}*$ (Eq. (7)) on temperature at infinite dilution in Fe metal compared to lower T data from the literature (note that the data span a range of f_{O_2} and P conditions). Error bars are positive and negative ranges on $D_{Pt}^{met/sil}*$ within one standard error ($\pm\sigma_M$) of the mean.

is more useful than across buffers at constant f_{O_2}. Thus, unlike the other studies presented in Fig. 6 that normalize results to a single f_{O_2} (± temperature), our values for $\log D_{Pt}^{met/sil}*$ correct only for activity–composition relationships. A trend toward increasing solubility (falling $D_{Pt}^{met/sil}*$) with increasing T can be discerned from Fig. 6. The fact that Pt solubility increases with increasing T at constant absolute f_{O_2} has been demonstrated over a 250 °C temperature range (1300–1550 °C) by Fortenfant et al. (2003), though the effect measured here appears to be much greater than extrapolation from that T range predicts, as discussed in Section 4.2.

Our calculated $D_{Pt}^{met/sil}*$ are even more remarkable in light of the experimental f_{O_2}, enforced through the use of graphite capsules, that lies near or below the iron–wüstite buffer as estimated from ΔIW and observed reduction of $FeO_{silicate} \to Fe_{metal}$. All previous interpretations of Pt solubility experiments suggest that Pt solubility should fall as f_{O_2} drops. In contrast, we do not measure an increase in $D_{Pt}^{met/sil}*$ with decreasing relative f_{O_2}. Of course, variations in T complicate this trend. When experiments run only at 2000 °C are compared, however, we still do not measure an increase in $D_{Pt}^{met/sil}*$ with falling f_{O_2}. We attribute this f_{O_2} insensitivity (here and in the other studies) to the presence of neutrally speciated Pt in the melt, whose solubility would be independent of changes in f_{O_2}.

5. Discussion

If interactions between metal and silicate were similar during core formation to those seen here experimentally (correcting for activity–composition relationships), then Pt must have entered the silicate of the magma ocean in much greater quantities than previously believed during core formation.

Using our values for $D_{Pt}^{met/sil}*$ it is possible to calculate the expected mantle depletion of Pt relative to C1 chondrites according to:

$$X_{LS}^{Pt} = \frac{X_{C1}^{Pt}}{[x + (1-x)(D_{Pt}^{met/sil})]}, \quad (8)$$

where x is the silicate fraction of Earth (=0.68) and X_{C1}^{Pt} is the chondritic Pt abundance = 1010 ppb (McDonough and Sun, 1995). We calculate an expected mantle Pt abundance (X_{LS}^{Pt})of 0.01–0.1 ppb. Primitive mantle Pt abundances average 7.1 ppb as reported by McDonough and Sun (1995). Equilibration between metal and silicate in a putative magma ocean may therefore nearly reconcile predicted and observed mantle Pt abundances, as they do for the MSE (Fig. 7).

The $D_{Pt}^{met/sil}*$ values we calculate are similar to those calculated for Re by Righter and Drake (1997); however,

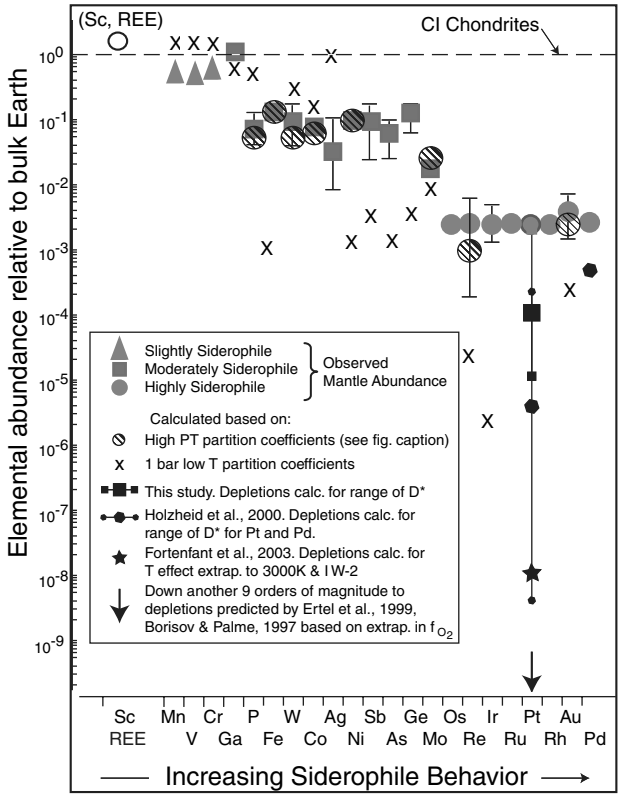

Fig. 7. Elemental mantle abundances relative to CI chondrite. Shaded solid symbols show observed upper mantle abundances, crosses represent calculated abundances based on experiments at low pressure and temperature (data from Newsom, 1990; Newsom et al., 1996; Capobianco et al., 1993). Calculated depletions based on experiments at low pressure and temperature do not quantitatively reproduce the observed upper mantle abundances; however, the effect of high pressure and temperature on $D_i^{met/sil}$, and hence on calculated siderophile element depletions relative to CI chondrites, can reconcile this difference for the moderately siderophile elements. Hatched dots reflect estimated depletions in a magma ocean: MSE depletions are from Righter et al. (1997), Righter and Drake (1999), Walter et al. (2000), Chabot et al. (2005), Re from Righter and Drake (1997) based on multiple linear regression of Re partitioning studies (though this data is controversial (Ertel et al., 2001)), and Au from Danielson et al. (2005). Other Pt data are from Holzheid et al. (2000), Fortenfant et al. (2003), Borisov and Palme (1997), Ertel et al. (1999) and are depicted as reported by those authors (i.e., assuming only divalent Pt). Solid black square represents calculated Pt abundance based on measured $D_{Pt}^{met/sil}$ under magma ocean-like conditions (this study). Figure adapted from Drake and Righter (2002).

$D_{Re}^{met/sil}$ has yet to be actually measured under magma ocean conditions. Ertel et al. (2001) heavily criticized the study by Righter and Drake (1997) and suggested values 6 orders of magnitude higher for $D_{Re}^{met/sil}$. Again, the controversy has its roots in the extrapolation to the reducing conditions of core formation, with Righter and Drake (1997) assuming Re^{2+} and Ertel et al. (2001) assuming Re^{4+} or Re^{6+}. The wildly divergent values for $D_{Re}^{met/sil}$ boil down to differences in nugget interpretation which remains an unresolved issue for Re.

Calculated $D_{Pd}^{met/sil}$ based on measurements by Holzheid et al. (2000) seem consistent with Pd's budget having been set by metal–silicate equilibrium in a magma ocean. Holzheid et al. (2000) report $D_{Pd}^{met/sil}* = 2.5 \times 10^5$ (and measure $D_{Pd}^{met/sil} = 6.2 \times 10^3$) at 1550 °C, 15.5 GPa, and with extrapolation to IW − 2.5 (thus assuming only monovalent Pd). When they add the temperature dependence for Pd partitioning determined by Borisov et al. (1994) (≈1.63 orders of magnitude), $D_{Pd}^{met/sil}*$ drops to 8×10^3. These experiments predict a mantle Pd depletion equal to 3.9×10^{-4}—less than one order of magnitude lower than the observed mantle depletion.

Danielson et al. (2005) report $D_{Au}^{met/sil} = 100 - 2.65 \times 10^4$ with a preferred value of 1×10^3 for a magma ocean scenario ($T = 2127$ °C, $P = 27$ GPa, $\Delta IW = -2.3$, nbo/$T = 2.65$, $X_S = 0.9$). $D_{Au}^{met/sil}$ may therefore be consistent with equilibration in a magma ocean as well.

The mantle depletions of Pt, Pd, Au, and perhaps Re may be consistent with those expected from metal–silicate equilibration in a magma ocean. Many hurdles remain, however, for an equilibrium model to account for the entire suite of mantle siderophile element budgets. The partition coefficients of Ir, Os, Ru, Rh, and Ag must not only drop relative to those measured under low pressure–temperature conditions, but they must also converge if their modern mantle chondritic ratios are representative of those set by an early magma ocean. In the case of Re and Os, isotopic evidence indicates a long-standing chondritic ratio (e.g., Meisel et al., 1996). The influence of many additional parameters on HSE partitioning, such as sulfur fugacity, the identity of the light element in the core, and the presence or absence of water or other volatiles, also has yet to be determined. So too does an exploration of the effect of P from 25 to 60 GPa, the likely range of pressures in a magma ocean as predicted by studies of the moderately siderophile elements (Gessmann and Rubie, 2000; Li and Agee, 2001; Chabot et al., 2005). It remains to be seen what effect these parameters will have. Efforts to parameterize the growing experimental space, such as has been done by Righter (2003), will benefit from studies that investigate variables in isolation and avoid large extrapolations.

6. Conclusions

We measure Pt solubilities at temperatures between 2000 and 2500 °C, at 2.2 GPa, under reducing f_{O_2}, and for prim-

itive Fe-bearing compositions. Although the data in this study, as in all studies at low f_{O_2}, display a wider scatter than can be attributed to analytical uncertainty, we conclude as our central result that Pt solubility in silicate is much higher than previous studies have measured or assumed and that Pt micro-nuggets may nucleate upon thermal quench. Our measurements suggest $D_{Pt}^{met/sil}$ of $\approx 10^{4-6}$ at infinite dilution in iron metal during core segregation and that equilibrium between metal and silicate in a hot magma ocean may in large have set the Pt budget of the modern mantle.

Acknowledgments

The authors would like to thank Charles Mandeville, Robert Fogel, and Rick Mortlock for technical assistance and Jill Pasteris for generously analyzing our samples with Raman spectroscopy. We also thank Tim Grove and Herb Kellogg for useful comments, Beth Gier for assistance with the LA-ICPMS, and Kevin Wheeler for sharing his pressure calibration. We gratefully acknowledge helpful reviews from H. Palme, A. Borisov, A. Holzheid, and Nancy Chabot. We also thank GCA editor F.J. Ryerson. This work was supported by the NSF and the American Association of University Women. This is LDEO contribution number 6842.

Associate editor: F.J. Ryerson

Appendix A. Supplementary data

Supplementary data associated with this article can be found, in the online version, at doi:10.1016/j.gca.2005.11.021.

References

Benz, W., Cameron, A.G.W., 1990. Terrestrial effects of the giant impact. In: Newsom, H.E., Jones, J. (Eds.), *Origin of the Earth*. Oxford Press, New York, pp. 61–68.

Borisov, A., Palme, H., 1995. The solubility of iridium in silicate melts—new data from experiments with $Ir_{10}Pt_{90}$ alloys. *Geochimica et Cosmochimica Acta* **59** (3), 481–485.

Borisov, A., Palme, H., 1997. Experimental determination of the solubility of platinum in silicate melts. *Geochimica et Cosmochimica Acta* **61** (20), 4349–4357.

Borisov, A., Palme, H., Spettel, B., 1994. Solubility of palladium in silicate melts—implications for core formation in the Earth. *Geochimica et Cosmochimica Acta* **58** (2), 705–716.

Cameron, A.G.W., 2002. Planetary science—birth of a solar system. *Nature* **418** (6901), 924–925.

Canup, R.M., Asphaug, E., 2001. Origin of the moon in a giant impact near the end of the Earth's formation. *Nature* **412** (6848), 708–712.

Capobianco, C.J., Jones, J.H., Drake, M.J., 1993. Metal-silicate thermochemistry at high-temperature—magma oceans and the excess siderophile element problem of the Earths upper mantle. *Journal of Geophysical Research-Planets* **98** (E3), 5433–5443.

Chabot, N.L., Agee, C.B., 2003. Core formation in the Earth and moon: new experimental constraints from V, Cr, and Mn. *Geochimica et Cosmochimica Acta* **67** (11), 2077–2091.

Chabot, N.L., Draper, D.S., Agee, C.B., 2005. Conditions of core formation in the earth: Constraints from nickel and cobalt partitioning. *Geochimica et Cosmochimica Acta* **69** (8), 2141–2151.

Chase, M., 1998. NIST-JANAF Thermochemical Tables, fourth ed., vol. Monograph 9. National Institute of Standards Technology.

Cottrell, E., 2004. Differentiation of the earth from the bottom up: Core, lithosphere, and crust. Ph.D. thesis, Columbia University.

Cottrell, E., Walker, D., 2002. A new look at Pt solubility in silicate liquid. In: *Proc. 33rd Lunar Planet. Sci. Conf*. Abs no. 1274.

Cottrell, E., Walker, D., 2004. Ultra-high temperature effects in a magma ocean: Pt and W partitioning. In: Jones, J., Herd, C. (Eds.), *Oxygen in Terrestrial Planets*. Lunar and Planetary Institute, Santa Fe, NM.

Danielson, L., Sharp, T., Hervig, R.L., 2005. Implications for core formation of the Earth from high pressure–temperature Au partitioning experiments. In: *Proc. 36th Lunar and Planet. Sci. Conf*. Abs no. 1955.

Dixon, J.E., Stolper, E., Delaney, J.R., 1988. Infrared spectroscopic measurements of CO_2 and H_2O in Juan-de-Fuca ridge basaltic glasses. *Earth and Planetary Science Letters* **90** (1), 87–104.

Drake, M.J., Righter, K., 2002. Determining the composition of the Earth. *Nature* **416** (6876), 39–44.

Ertel, W., O'Neill, H.S., Sylvester, P.J., Dingwell, D.B., 1999. Solubilities of Pt and Rh in a haplobasaltic silicate melt at 1300 degrees C. *Geochimica et Cosmochimica Acta* **63** (16), 2439–2449.

Ertel, W., O'Neill, H.S., Sylvester, P.J., Dingwell, D.B., Spettel, B., 2001. The solubility of rhenium in silicate melts: Implications for the geochemical properties of rhenium at high temperatures. *Geochimica et Cosmochimica Acta* **65** (13), 2161–2170.

Fortenfant, S.S., Gunther, D., Dingwell, D.B., Rubie, D.C., 2003. Temperature dependence of Pt and Rh solubilities in a haplobasaltic melt. *Geochimica et Cosmochimica Acta* **67** (1), 123–131.

Gessmann, C.K., Rubie, D.C., 1998. The effect of temperature on the partitioning of nickel, cobalt, manganese, chromium, and vanadium at 9 GPa and constraints on formation of the Earth's core. *Geochimica et Cosmochimica Acta* **62** (5), 867–882.

Gessmann, C.K., Rubie, D.C., 2000. The origin of the depletions of V, Cr and Mn in the mantles of the Earth and moon. *Earth and Planetary Science Letters* **184** (1), 95–107.

Gudmundsson, G., Holloway, J.R., 1993. Activity-composition relationships in the system Fe-Pt at 1300 °C and 1400 °C and at 1-atm and 20-Kbar. *American Mineralogist* **78** (1-2), 178–186.

Halliday, A.N., 2004. Mixing, volatile loss and compositional change during impact-driven accretion of the Earth. *Nature* **427** (6974), 505–509.

Hillgren, V.J., Drake, M.J., Rubie, D.C., 1994. High-pressure and high-temperature experiments on core-mantle segregation in the accreting Earth. *Science* **264** (5164), 1442–1445.

Holzheid, A., Palme, H., Chakraborty, S., 1997. The activities of NiO, CoO and FeO in silicate melts. *Chemical Geology* **139** (1–4), 21–38.

Holzheid, A., Sylvester, P., O'Neill, H.S.C., Rubie, D.C., Palme, H., 2000. Evidence for a late chondritic veneer in the Earth's mantle from high-pressure partitioning of palladium and platinum. *Nature* **406** (6794), 396–399.

Huebner, J., 1972. Buffering techniques for hydrostatic systems at elevated pressures. In: Ulmer, G. (Ed.), *Research Techniques for High Pressure and High Temperature*. Springer, New York.

Hultgren, R., Desai, P., Hawkins, D., Gleisen, M., Kelley, K., 1971. Fe-Pt binary alloy. In: *Selected Values of the Thermodynamic Properties of Binary Alloys Part 2*. American Society for Metals, Materials Park, OH, pp. 861–865.

Karato, S., Murthy, V.R., 1997. Core formation and chemical equilibrium in the Earth .1. Physical considerations. *Physics of the Earth and Planetary Interiors* **100** (1-4), 61–79.

Kegler, P., Holzheid, A., Rubie, D.C., Frost, D.J., Palme, H., 2004. Reinvestigation of the Ni and Co metal–silicate partitioning. In: *Proc. 35th Lunar and Planet. Sci. Conf*. Abs no. 1632.

Kegler, P., Holzheid, A., Rubie, D.C., Frost, D.J., Palme, H. 2005. New results of metal/silicate partitioning of Ni and Co at elevated pressures

and temperatures. In: *Proc. 36th Lunar and Planet. Sci. Conf*. Abs no. 2030.

Kimura, K., Lewis, R.S., Anders, E., 1974. Distribution of gold and rhenium between nickel-iron and silicate melts—implications for abundance of siderophile elements on Earth and moon. *Geochimica et Cosmochimica Acta* **38** (5), 683–701.

Li, J., Agee, C.B., 1996. Geochemistry of mantle-core differentiation at high pressure. *Nature* **381** (6584), 686–689.

Li, J., Agee, C.B., 2001. The effect of pressure, temperature, oxygen fugacity and composition on partitioning of nickel and cobalt between liquid Fe-Ni-S alloy and liquid silicate: Implications for the Earth's core formation. *Geochimica et Cosmochimica Acta* **65** (11), 1821–1832.

Lindstrom, D.J., Jones, J.H., 1996. Neutron activation analysis of multiple 10–100 μg glass samples from siderophile element partitioning experiments. *Geochimica Et Cosmochimica Acta* **60** (7), 1195–1203.

Lux, G., 1987. The behavior of noble-gases in silicate liquids—solution, diffusion, bubbles and surface effects, with applications to natural samples. *Geochimica et Cosmochimica Acta* **51** (6), 1549–1560.

McDonough, W.F., Sun, S.S., 1995. The composition of the Earth. *Chemical Geology* **120** (3-4), 223–253.

Meisel, T., Walker, R.J., Morgan, J.W., 1996. The osmium isotopic composition of the earth's primitive upper mantle. *Nature* **383** (6600), 517–520.

Mills, K., 1993. The influence of structure on the physico-chemical properties of slags. *ISIJ International* **33**, 148–155.

Murthy, V.R., 1991. Early differentiation of the Earth and the problem of mantle siderophile elements—a new approach. *Science* **253** (5017), 303–306.

Newsom, H.E., 1990. Accretion and core formation in the Earth: Evidence from siderophile elements. In: Newsom, H.E., Jones, J. (Eds.), *Origin of the Earth*. Oxford University Press, Oxford, pp. 273–288.

Newsom, H.E., Sims, K.W.W., Noll, P.D., Jaeger, W.L., Maehr, S.A., Beserra, T.B., 1996. The depletion of tungsten in the bulk silicate Earth: Constraints on core formation. *Geochimica et Cosmochimica Acta* **60** (7), 1155–1169.

O' Neill, H.S., 1991. The origin of the moon and the early history of the Earth—a chemical-model. 2. the Earth. *Geochimica et Cosmochimica Acta* **55** (4), 1159–1172.

O' Neill, H.S.C., Dingwell, D.B., Borisov, A., Spettel, B., Palme, H., 1995. Experimental petrochemistry of some highly siderophile elements at high temperatures, and some implications for core formation and the mantles early history. *Chemical Geology* **120** (3-4), 255–273.

Righter, K., 2003. Metal-silicate partitioning of siderophile elements and core formation in the early Earth. *Annual Review in Earth Planetary Science* **31** (1), 135–174.

Righter, K., Drake, M.J., 1997. Metal-silicate equilibrium in a homogeneously accreting earth: New results for Re. *Earth and Planetary Science Letters* **146** (3-4), 541–553.

Righter, K., Drake, M.J., 1999. Effect of water on metal–silicate partitioning of siderophile elements: a high pressure and temperature terrestrial magma ocean and core formation. *Earth and Planetary Science Letters* **171** (3), 383–399.

Righter, K., Drake, M.J., Yaxley, G., 1997. Prediction of siderophile element metal–silicate partition coefficients to 20 GPa and 2800 degrees C: The effects of pressure, temperature, oxygen fugacity, and silicate and metallic melt compositions. *Physics of the Earth and Planetary Interiors* **100** (1–4), 115–134.

Ringwood, A.E., 1966. Chemical evolution of the terrestrial planets. *Geochimica et Cosmochimica Acta* **30**, 40–104.

Ringwood, A.E., 1979. *Origin of the Earth and Moon*. Springer, New York.

Rubie, D.C., Melosh, H.J., Reid, J.E., Liebske, C., Righter, K., 2003. Mechanisms of metal–silicate equilibration in the terrestrial magma ocean. *Earth and Planetary Science Letters* **205** (3-4), 239–255.

Sasaki, S., Nakazawa, K., 1986. Metal-silicate fractionation in the growing Earth—energy-source for the terrestrial magma ocean. *Journal of Geophysical Research-Solid Earth and Planets* **91** (B9), 9231–9238.

Stevenson, D., 1990. Fluid dynamics of core formation. In: Newsom, H.E., Jones, J. (Eds.), *Origin of the Earth*. Oxford University Press, New York, pp. 231–249.

Stolper, E., Holloway, J.R., 1988. Experimental-determination of the solubility of carbon-dioxide in molten basalt at low-pressure. *Earth and Planetary Science Letters* **87** (4), 397–408.

Su, Y.J., 2002. Mid-ocean ridge basalt trace element systematics: Constraints from database management, ICP-MS analyses, global data compiliation, and petrologic modeling. Ph.D., Columbia University.

Sylvester, P.J., Eggins, S.M., 1997. Analysis of Re, Au, Pd, Pt and Rh in NIST glass certified reference materials and natural basalt glasses by laser ablation ICP-MS. *Geostandards Newsletter-The Journal of Geostandards and Geoanalysis* **21** (2), 215–229.

Thibault, Y., Walter, M.J., 1995. The influence of pressure and temperature on the metal–silicate partition-coefficients of nickel and cobalt in a model-cl chondrite and implications for metal segregation in a deep magma ocean. *Geochimica et Cosmochimica Acta* **59** (5), 991–1002.

Walker, D., Norby, L., Jones, J.H., 1993. Superheating effects on metal–silicate partitioning of siderophile elements. *Science* **262** (5141), 1858–1861.

Walter, M.J., Newsom, H.E., Ertel, W., Holzheid, A., 2000. Siderophile elements in the Earth and moon: metal/silicate partitioning and implications for core formation. In: Canup, R., Righter, K. (Eds.), *Origin of the Earth and Moon*. University of Arizona Press, Cambridge, pp. 265–290.

Walter, M.J., Tronnes, R.G., 2004. Early Earth differentiation. *Earth and Planetary Science Letters* **225** (3–4), 253–269.

Wänke, H., 1981. Constitution of terrestial planets. *Philosophical Transactions of the Royal Society of London Series A-Mathematical Physical and Engineering Sciences* **303** (1477), 287–302.

Yoshino, T., Walter, M.J., Katsura, T., 2003. Core formation in planetesimals triggered by permeable flow. *Nature* **422** (6928), 154–157.